Environmental Science and Pollution Research
https://doi.org/10.1007/s11356-024-34988-y

RESEARCH ARTICLE

New spacious $SrWO_4$/PEDOT-PPy nanohybrids and their electrochemical and photocatalytic activities

Settu Munusamy[2] · Gnanamoorthy Govindhan[1,3] · Ziyang Lu[1] · Jie Jin[1]

Received: 10 July 2024 / Accepted: 11 September 2024

Abstract

A novel $SrWO_4$-poly(3,4-ethylene dioxythiophene) (PEDOT)-polypyrrole (PPy) nanocomposite was synthesized via chemically oxidative polymerization and considered by using numerous method of the techniques. The resulting $SrWO_4$/PEDOT-PPy nanocomposite demonstrated remarkable electrochemical sensing capabilities for sulfadiazine (SFA). As a modified glassy carbon electrode ($SrWO_4$/PEDOT-PPy/GCE) revealed for superior catalytic activity in the electrochemical oxidation of sulfadiazine, enabling sensitive detection with quantification and detection limits of 1.0936×10^{-9} M μA^{-1} and 2.2104×10^{-9} M μA^{-1}, respectively. This technique effectively determined SFA content in real samples. Additionally, $SrWO_4$/PEDOT-PPy demonstrated extraordinary photocatalytic ability, achieving a Methylene Blue (MB) degradation rate of up to 99.1% under halogen light irradiation within 80 min. Hybrid photocatalyst has exhibited to strong reusability and photocatalytic stability under frequent light exposure. A contrivance for the photocatalytic deprivation of MB by $SrWO_4$/PEDOT-PPy is proposed. These results underscore the crucial role of $SrWO_4$/PEDOT-PPy in practical environmental remediation analysis. The fluorescence investigations have betrothed to terephthalic acid radical formations of $SrWO_4$/PEDOT-PPy hybrids, which were modulated by different approaches, and its mainly driven for higher illumination aptitudes. Meanwhile, this was more supporting for physio-chemical properties of the phenomenon, at this consequential with significantly well improved to the photocatalytic performances. Because of this, $SrWO_4$/PEDOT-PPy hybrid materials were comprehended to deliver excellent kinetics, and better recyclable activities.

Keywords $SrWO_4$ nanoparticles · PEDOT-PPy hybrids · Sulfadiazine (SFA) · MB

Introduction

Nanostructured conducting polymers represent an emerging class of materials characterized by their unique mechanical, electrical, and optical properties. This nanocatalysts encompass various conducting polymers, including polyaniline, polypyrrole (PPy), polythiophene, and their by-products (Wang et al. 2022; Ramanavicius and Malinauskas 2006; Shuying and Stephen 2006; Karlsson et al. 2005, Kang et al. 2004). Recently, various morphologies have been reported, such as films with microspores, hollow, micro, nanospheres, nanotubes, and nanofibers. These morphologies contribute to conducting polymers diverse electronic and optical properties, which can be further enhanced by molecular arrangement or incorporating other organic and inorganic materials. The poly(3,4-ethylenedioxythiophene) (PEDOT) stands for an extreme conductance that can be produced via oxidative polymerization or electrochemical polymerization (Parthasarathy et al. 1994; Jia et al. 2024; Yang, et al. 2024; Zhang et al. 2006). It has been found that the applications in antistatic coatings and organic light-emitting devices have been achieved by an excellent conductivity and π-conjugated structure. Similarly, PPy exhibits good electrical conductivity and environmental stability, assembling for appropriate applications like electronic and

Responsible Editor: George Z. Kyzas

Settu Munusamy and Gnanamoorthy Govindhan are co-first authors.

✉ Gnanamoorthy Govindhan
gnanadrdo@gmail.com

[1] School of Environment and Safety Engineering, Jiangsu University, Zhenjiang 212013, Jiangsu, China

[2] Centre for Applied Nanomaterials, Chennai Institute of Technology, Chennai 600069, Tamil Nadu, India

[3] Department of Inorganic Chemistry, University of Madras, Chennai 600025, Tamil Nadu, India

Published online: 19 September 2024

optical devices, electrochemical sensors, and field emission applications. PPy nanomaterials were frequently dealing with different methods, such as complicated porous polymeric templates, electro-spinning, interfacial polymerization, and surfactant-assisted micelles. Surfactants or doping agents are crucial in directing reaction pathway for specific sizes and shapes of nanomaterials. Moreover, performance of sensors has been utilizing polymerization on the system phases, emphasizing importance in comprehensively understanding and meticulously controlling for the materials composition and morphologies. The PEDOT-PPy is an organic hybrid material that exhibits several desirable applications in various fields. These materials may be due to its high conducting and excellent environmental stability (Shim et al. 2008; Peng et al. 2007; Groenendaal et al. 2000; Wallace and Kane-Maguire 2002). The efficiency of sensors utilizing polymers relies on numerous factors with phase transition also significantly valid. Therefore, we have selected for Sr-based tungsten oxide ($SrWO_4$), which are exhibited to an extensively tunable band gaps, typically in the ranges at 2.3 to 2.8 eV (Berdichevsky and Lo 2006; Otero and Cortes 2003; Wang and Jiang 2000). These $SrWO_4$ consume harvested important consideration due to their versatile activities with wide a range of applications. The $SrWO_4$ thin films and nanoparticles have been widely studied and tested by the microelectronics and catalysis scenarios (Pringle et al. 2004; Wang and Martin 1996; Kang et al. 2005; Vito and Martin 1998; Jang and Yoon 2005). Additionally, $SrWO_4$ has been explored by devices that serve as a photoanode material to convert solar energy into electricity (Goren and Lennox 2001; Wu et al. 2005; De Armit and Armes 1993; Eftekhari and Kazemzad 2006). $SrWO_4$ nanoparticles can be incorporated as electron transport layers in colloidal quantum dot LEDs to improve device performance. Consequently, photocatalysis and photoelectron catalysis are other vital crucial roles (Zhang and Manohar 2004; Chen et al. 2011; Kumar et al. 2016; Raja et al. 2019; Jiandong et al. 2006; Bingyu et al. 2016). $SrWO_4$-based photocatalysts have shown promise in various environmental applications, including water splitting like hydrogen production and methanol oxidation for fuel cells. Other than those, notable application is wastewater treatment, where $SrWO_4$ serves as a visible light photocatalyst to generate highly reactive hydroxyl radicals ($OH^{\bullet}$). $SrWO_4$ is a versatile material with diverse applications across different fields, from electronics and catalysis to environmental remediation (Yu et al. 2024; Altunay 2022). The innovative points of the work, this material has a new creative movement of double layers polymerization, and it should be monitored for the first time addressed, to be examined for good capabilities in electrochemical sensing with enhanced to the higher active sites. Not only that, it's an effort to photocatalytic degradation applications. Similar kinds of reports have been engaged in the past few days. The tunable band gap, semiconductor properties, and photocatalytic activity make it a promising candidate for addressing various technological and ecological challenges. Moreover, incorporating PEDOT-PPy into $SrWO_4$ conducting polymers can alter the phase transition state of $SrWO_4$, leading to significant effects on sensor activity. This composite formation, such as $SrWO_4$/PEDOT-PPy to introduce p-n type characteristics, which can enhance the electrocatalytic and photocatalytic processes. $SrWO_4$ is combined with PEDOT-PPy and interaction between the two materials can transform the structural and electronic possessions of the composite. The PEDOT-PPy component being a conducting polymer, while introduces additional conductivity for the composite. Moreover, the presence of PEDOT-PPy can influence phase transition behaviour of $SrWO_4$ materials with potentially altering its crystalline structure and other phase composition. This modification of the phase transition state of $SrWO_4$ materials due to the accumulation of PEDOT-PPy nanohybrids has been achieved by several effects on sensor activity.

The different forms of the polymorphic materials can be performed in numerous physical and chemical properties, and then modern functionalities are also predicted (Rajkumar et al. 2023; Kokulnathan 2021; Shivakumara et al. 2015; Rendón-Angeles et al. 2015; Sczancoski et al. 2009). Note that, this $SrWO_4$ material has been acceptable for various advantages like less toxicity, low cost, higher surface capacitance, low bandgap energy, abundance, charge separations, mobility, stability, environment friendly, and economically good yields also and optimized in corresponding achievements. These criteria of the key points are more favourable to the material designation, improved the catalytic activities and globalized confirmations. For example, electrode interface, rapid reaction, surface active sites, and electron mobilities. Forever, these materials have been morphologically different because of synthetic approach that was potentially modified and rectified the new convergent activities with lead to the electrochemical sensing, and deliver the reliable photoelectron and further activities. This material is morphologically unclassified due to high dopant concentration and obeys for agglomeration which could not be achieved by any other demerits. All activities are more viable for the composite's formation. Firstly, it can improve the composites charge transport properties, enhancing for electrocatalytic activities. This result has enriched for more efficient sensing of analytes through electrochemical methods like cyclic voltammetry, etc. Additionally, the modified phase transition state of $SrWO_4$ in nanohybrids can be improved for the photocatalytic properties. Familiarizing $SrWO_4$/PEDOT-PPy hybrids can improve the photocatalytic activities in MB irradiation by modifying the electronic band structure or surface morphology of $SrWO_4$. These advancements pave the way for $SrWO_4$/PEDOT-PPy as highly effective sensors

capable for addressing various analytical challenges from environmental monitoring to healthcare diagnostics.

Experimental details

Material and methods

All the chemicals used in the experiments were obtained from reputable suppliers and used without further purification. Here are the listed chemicals and their respective suppliers: Camphor sulfonic acid-$C_{10}H_{16}O_4S$ (CSA), Strontium Nitrate ($Sr(NO_3)_2$), Ammonium persulfate ($(NH_4)_2S_2O_8$), Sodium tungstate dihydrate ($Na_2WO_4{\cdot}2H_2O$), Pyrrole (C_4H_4NH), EDOT (3,4-Ethylenedioxythiophene)-$C_2H_4O_2C_4H_2S$, Terephthalic acid ($C_8H_6O_4$), Sulfadiazine ($C_{10}H_{10}N_4O_2S$), Acetone, Chloroform, Ethanol, Ether, Ethyl acetate, and MB. All chemicals and reagents were procured by LR grade with Sigma Aldrich, and using to straight without any extra treatments.

Synthesis of $SrWO_4$ nanoparticles

Synthesis procedure for $SrWO_4$ involves the reaction between $Na_2WO_4{\cdot}2H_2O$ and $Sr(NO_3)_2$ under specific conditions. Typically, $Na_2WO_4{\cdot}2H_2O$ (1.65 g) was soluble in 100 mL of deionized water using an ultrasonicate for 40 min. This step helps in achieving the uniform dissolution of $Na_2WO_4{\cdot}2H_2O$. Additionally, (0.15 g) $Sr(NO_3)_2$ solution was mixed in the solution under the ultrasonication. This reaction mixture was continued with an ultrasonicator at 90 °C for 120 min (Alkaykh et al. 2020; Moztahida and Lee 2020; Shi et al. 2017). Furthermore, ultrasonicate has been maintained for 50 kHz frequency with 150 W of power control. After completion of the reaction, we can achieve the $SrWO_4$ colloidal precursor after being collected by centrifugation. The centrifuged product is then washed five times using a mixture of DD water and alcohol to remove impurities.

Synthesis of $SrWO_4$/PEDOT-PPy nanohybrids

The same procedure was applied for synthesizing $SrWO_4$/PEDOT-PPy nanohybrids. However, 0.10 g of $SrWO_4$ was added in 100 mL of DD water, while stirring condition, and this initial polymerization step was mentioned for ice cooling under being stirred. Then, 0.1 mL of CSA in 50 mL of solutions containing EDOT-CSA-pyrrole was separately supplementary of the concoction. This addition is monitored dropwise and followed by the gradual accumulation of $(NH_4)_2S_2O_8$ solution for synthesizing the $SrWO_4$/PEDOT-PPy nanohybrid mixtures that were stirred overnight at 0 °C, and colour combination has changed from yellowish brown to blue-green product consecutively. The product was filtered and eroded five times using chloroform and then vacuum-dried for 48 h.

Degradation of MB

We must depict the temporal evolution of MB degradation with 5×10^{-3}. Molar concentration. This photocatalytic method of study has been followed by the reported articles (Gnanamoorthy et al. 2024a; Gnanamoorthy et al. 2024b; Gnanamoorthy et al. 2022).

Electrocatalytic activity of SFA

Cyclic voltammetry, DPV and other supporting analysis were evidenced by modification for surface of the GCE by $SrWO_4$/PEDOT-PPy with its explored good conductance, and surface areas in electrode. Modified $SrWO_4$/PEDOT-PPy GCE electrode has significantly improved the sensitivity for SFA molecules. We can achieve the marvellous electrochemical sensing obtained for more efficient detection in SFA molecules.

Results and discussion

X-ray diffraction investigations

Figure 1a–b illustrates the X-ray diffraction (XRD) patterns of $SrWO_4$ and $SrWO_4$/PEDOT-PPy nanohybrids, providing insights into their crystallinity and structural characteristics. As observed, $SrWO_4$ nanomaterials XRD pattern results have a good crystalline nature, with distinct diffraction peaks corresponding to the tetragonal crystal systems. As observed, $SrWO_4$ major peaks are well matched for JCPDS card no: 89–2568 & 85–0587 (Cavalcante et al. 2013; Zhang et al. 2015b; Rajkumar et al. 2023). In Fig. 1b, the XRD pattern of $SrWO_4$/PEDOT-PPy nanohybrids reveals some modifications in peak intensities and positions are compared to pure $SrWO_4$. The presence of PEDOT-PPy hybrids on $SrWO_4$ leads to noticeable changes in diffraction peak intensities and slight shifts in peak positions towards lower angles, which has obeyed the interactions between $SrWO_4$ and PEDOT-PPy, and then leading to the crystalline structures of the hybrid material. The diffraction peaks 2θ-24 to 26° can be ascribed to the (020) planes (Chougule et al. 2011; Zhang et al. 2015a; Munusamy et al. 2019) and then due to their less crystallinity with conductive nature of polymer backbone (Herrmann et al. 2015; Ammam et al. 2010). Accumulation of PEDOT-PPy to $SrWO_4$ decreases the overall crystallinity, as evidenced by the shifting of diffraction peaks towards lower 2θ values. This result indicates that PEDOT-PPy hybrids steric hinders for the crystallization of $SrWO_4$ grains, that subsequently reduced the diffraction

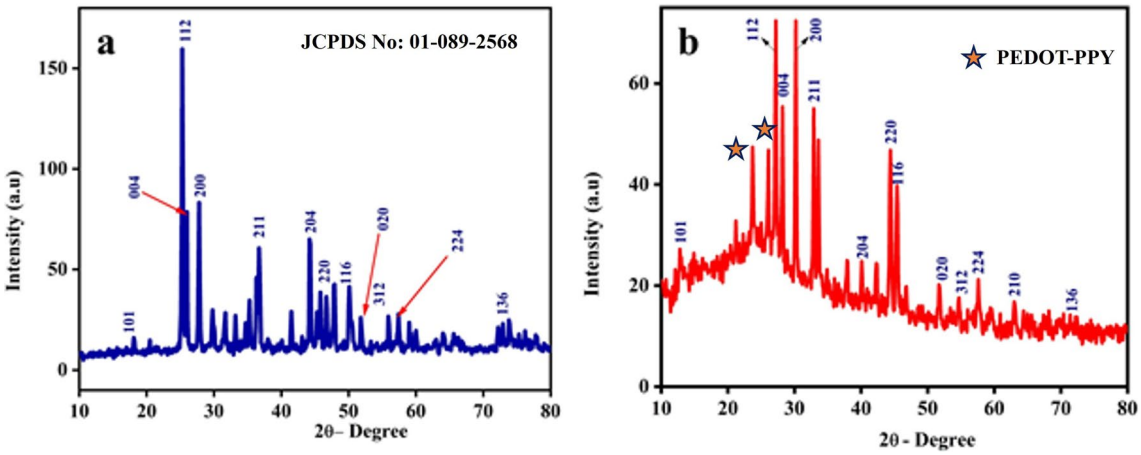

Fig. 1 **a**–**b** XRD investigations of $SrWO_4$ nanomaterials and (**b**) $SrWO_4$/PEDOT-PPy nanohybrid materials

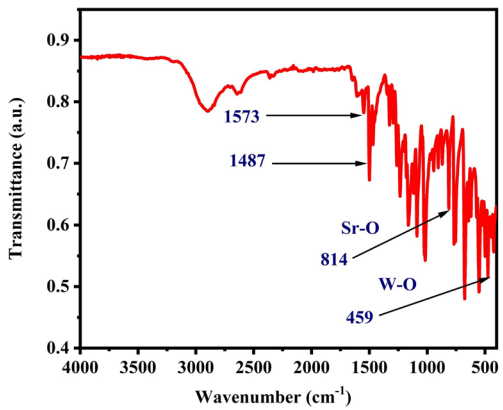

Fig. 2 FT-IR spectrum of (a) $SrWO_4$/PEDOT-PPy nanohybrid materials

peak intensities. The XRD analysis confirms the successful synthesis of $SrWO_4$/PEDOT-PPy nanohybrids and highlights the structural modifications to induced by the presence of conducting polymer on $SrWO_4$ materials with impacting on its crystallinity and peak characteristics.

FT-IR analysis

$SrWO_4$/PEDOT-PPy nanohybrids FT-IR result was shown in Fig. 2**.** The $SrWO_4$ nanoparticles display several bands. As determined and explained to that the several modes of the confirmation. The W–O antisymmetric stretching vibration as shown in band position is 814 cm^{-1}, besides peak 459 cm^{-1} predicted to Sr–O stretching vibrations (Suda and Zverev 2019). The peak 1092 cm^{-1} is corresponding to the C–O–C vibrations for methylenedioxy moieties and band 1566 cm^{-1} and 770 cm^{-1} ascribed to the thiophene-based functional molecules and C-S bond stretching vibrations of the molecules. Meanwhile, peak 1274 cm^{-1} agrees to the O = S = O (SO_2) widening vibrations that were present in PEDOT-PPy doped with CSA hybrids. The copolymer PEDOT-PPy exhibits three different significant peaks like 3785, 1450, and 1566 cm^{-1} due to intermolecular H-bonding and conjugation of the polymer's backbone. Furthermore, peak 3427 cm^{-1} and 3373 cm^{-1} for stretching vibrations for H–O-H and N–H moieties, respectively. This interaction has decreased wavenumber of the vibrational patterns that were detected even though indicating chemical interactions between $SrWO_4$ and PEDOT-PPy components.

UV–visible DRS spectroscopy investigations

$SrWO_4$/PEDOT-PPy nanohybrids DRS UV–visible absorption analysis were shown in Fig. 3a–b**.** This figure reveals strong absorption bands at 320 and 410 nm which signifies transition of optical infraction rings in $SrWO_4$/PEDOT-PPy nanohybrid materials. Furthermore, these bands are ascribed to π-π* transition in between poly-(3,4-ethylenedioxythiophene)-polypyrrole materials. Meanwhile, observed absorbance intensity has a longer wavelength which conferred to the red shift region of the $SrWO_4$/PEDOT-PPy nanohybrids. However, this does not appear in the peak shift, like arising from the electron–hole transition between $SrWO_4$ and PEDOT-PPy hybrids. $SrWO_4$/PEDOT-PPy materials band gap energy has been determined by Tauc equation from Kubelka- Monk function (given below).

$$(\alpha h\upsilon)^n = A(h\upsilon - Eg)^n$$

where, h is a Planck's constant, α is Absorption coefficient, υ is a Frequency and n is a 2 1/2 (direct and indirect) and A is a Constant.

Figure 3b demonstrates in between $(\alpha h\nu)^n$ and hu relationship for the $SrWO_4$/PEDOT-PPynanohybrids. As the determined bandgap energy value is 2.1 eV, supplementary can

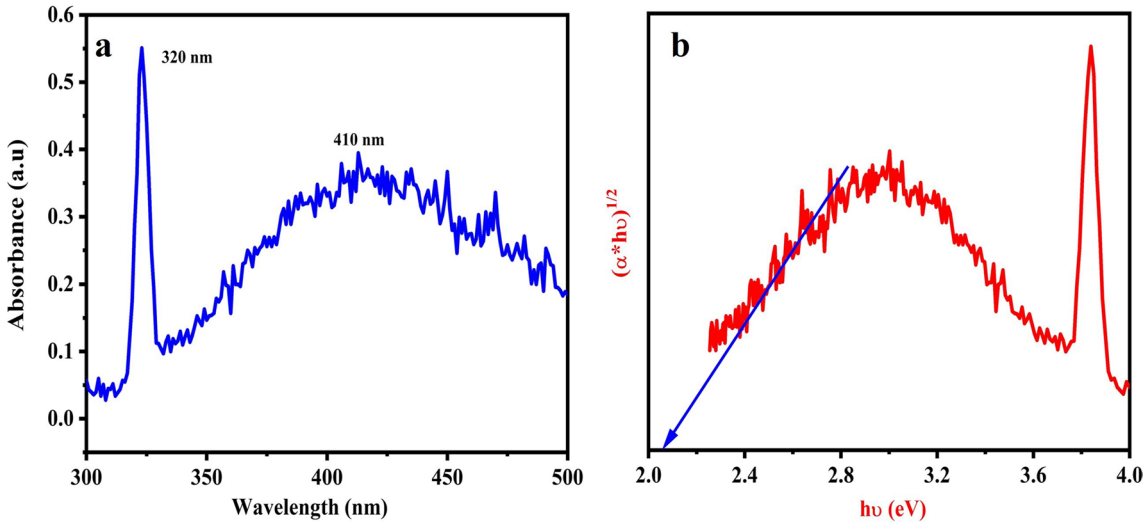

Fig. 3 **a**–**b** UV Visible DRS analysis: (**a**) $SrWO_4$ nanoparticles; (**b**) $SrWO_4$/PEDOT-PPy nanohybrid materials

occur to the correlation of the size. Which also obsessed and depends on quantum confinement effects. $SrWO_4$/PEDOT-PPynanohybrids observed below 450 nm ranges, it might be a low bandgap energy because this quantum confinement is sensible, and obtained results are suitable with referred other findings (Jayakrishnan et al 2024; Gnanamoorthy et al 2020). Furthermore, lattice strain, crystal defects, and other characters were also caused by the electronic band structure variations, then material energy levels were affected (Duraimurugan et al. 2018). In the future, the bandgap energy will be obeyed for the shifts, for the meantime this may be due to the molecular absorption on the surface being formed. The observed lower band gap energy results are more feasible for photocatalytic activity degradation applications.

Morphological analysis

Figures 4 and 5a–d presents FE-SEM and HR-TEM images of the $SrWO_4$ and $SrWO_4$/PEDOT-PPy nanohybrids. In Fig. 4a–c, the cubic shape of $SrWO_4$ nanoparticles can be observed. These nanoparticles appear uniformly sized with a diameter range of 0.5 to 1 µm. In Fig. 5a–c**,** the agglomerates consist of core–shell structures, indicating the presence of $SrWO_4$/PEDOT-PPy nanohybrids. The irregular cubic particles of $SrWO_4$ nanoparticles are clearly visible with agglomerates form of the morphology. Overall, the morphological images can illustrate to the successful synthesis of $SrWO_4$ nanoparticles and their integration of PEDOT-PPy nanohybrids achieved by the distinctive core–shell morphologies with ranges at 500 to 200 nm. $SrWO_4$/PEDOT-PPy hybrid has a core shell-like morphology, with appearance images of the PEDOT-PPy hybrid portraying the deposition of $SrWO_4$ nanoparticles using the chemical oxidative method. $SrWO_4$/PEDOT-PPy images sequence hybrid exposes a growth in the statement of $SrWO_4$ with a growth of polymerization, while creating a core–shell-type superficial construction. $SrWO_4$ over PEDOT-PPy delivers supreme synergistic sites. In place of polymerization classifications increase, the quantity of synergistic sites controls as $SrWO_4$ nanoparticles commence towards detach as a result of particle aggregation. Figure 5d portrays EDX spectrum of the $SrWO_4$ and PEDOT-PPy materials, which confirms the O, W, Sr elements and the C, and S elements are confirmed by PEDOT-PPy hybrids.

In Fig. 6a–c**,** the images depict $SrWO_4$ nanoparticles with PEDOT-PPy integrated onto their surface. The spherical structures have a length ranging from approximately 50 nm, 100 nm, and 200 nm. Its exhibits to be contributed and two-dimensional core–shell structures also formed in the hybrid materials. Moreover, the lattice fringes were also carefully examined by this investigation, which were shown in Fig. 6d. Furthermore, resulting images have indicated the atomic spacing of interplanar fringes at 0.3 nm and which ascribed to $SrWO_4$/PEDOT-PPy nanohybrids. Moreover, this relevant information has been followed by the specific records (Bu et al. 2024; Cheng et al. 2023).

Electrochemical behaviours of $SrWO_4$/PEDOT-PPy GCE

The $SrWO_4$/PEDOT-PPy/GCE electrode elaborate for dispersion of nanohybrids with sonication for 50 mL of Ethanol (0.1 mg/mL) and sulfadiazine (SFA) solution also prepared. The modified GCE was polished by 1500 emery sheet by sonication under ethanol cleaning, after modification of GCE. The modified GCE was further treated

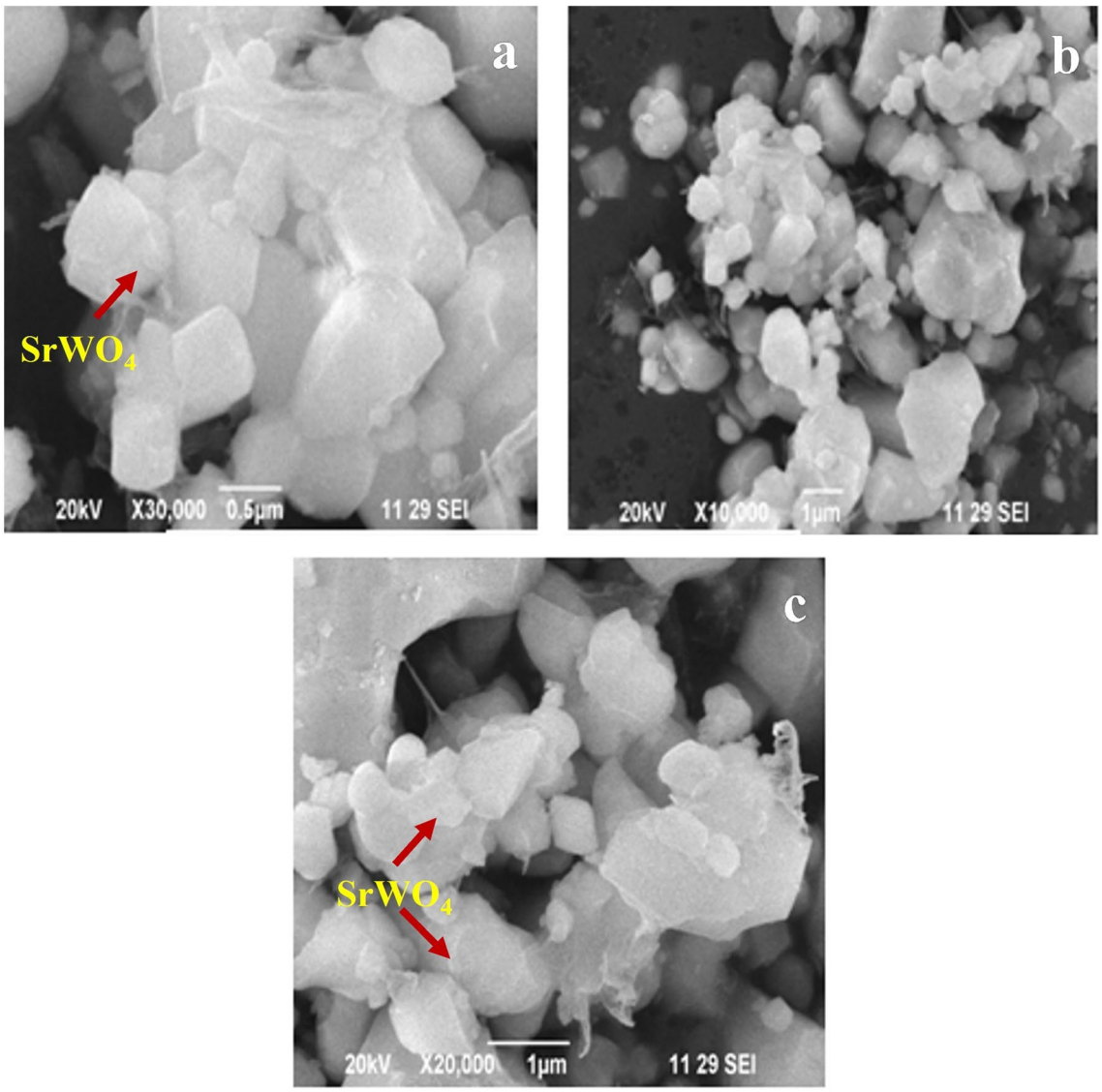

Fig. 4 **a–c** FE-SEM images of $SrWO_4$ nanoparticles

by immersing and then air-dried. These steps were crucial in creating an optimized $SrWO_4$/PEDOT-PPy/GCE electrode with improved properties for the electrochemical determination of SFA. Figure 7 explains the cyclic voltammetry curves of $SrWO_4$/PEDOT-PPy/GCE in the presence of the pH-6 and the optimum scan rate at 50 mVs^{-1}. CV of SFA at the modified GCE exhibits a prominent oxidation peak at around 0.95 V. The oxidation peaks of SFA at the $SrWO_4$/PEDOT-PPy modified GCE appears at a higher potential (0.95 V) compared to the bare GCE, indicating enhanced electron transfer kinetics facilitated by the modified GCE electrode. Thereafter, the anodic peak potential has been shifted towards the positive track by approximately 250 mV for the $SrWO_4$/PEDOT-PPy modified electrode, indicating its electrocatalytic ability. The $SrWO_4$/PEDOT-PPy/GCE shows a higher anodic peak current (1.5621 µA) and higher peak potential at + 0.95 V, compared to bare electrodes, while determined to its superior electrochemical sensing behavior, which corresponds to the core-shaped morphology of the $SrWO_4$/PEDOT-PPy nanohybrids, with a nanoscale size at 50 nm which has determined from HRTEM investigations, furthermore, contributes to enhancing electrochemical behaviors. It confirms the presence of surface functional groups like -NH-, -S-, -COO-, and redox of SFA sensor. Finally, we conclude that $SrWO_4$/PEDOT-PPy/GCE electrode has explored the well electrochemical sensing activities.

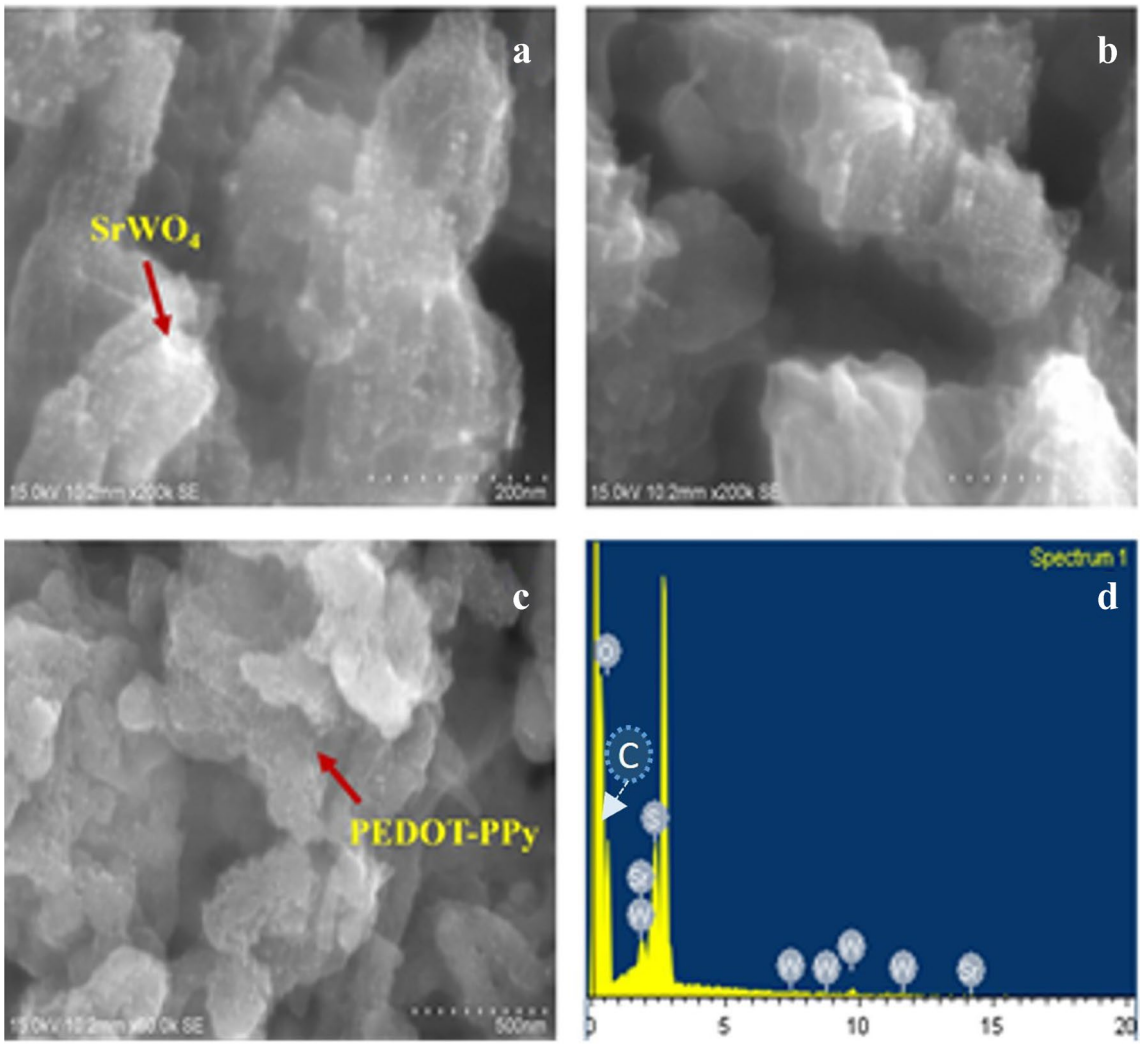

Fig. 5 **a**–**c** FE-SEM morphological images and (**d**) EDX spectrum of $SrWO_4$/PEDOT-PPy nanoparticles

Scan rate effects

Figure 8 shows scan rate of $SrWO_4$/PEDOT-PPy modified GCE in 0.1 mM SFA solution. However, oxidation peak potential is slightly changed towards higher values of the scan rate with increased peak potential, and then indicating the redox sites of the modified electrode and SFA. The anodic peak currents for SFA at the modified GC electrodes exhibited a linear relationship and the scan rate at 50–180 mVs^{-1}, and the calibration equation of $I(\mu A) = 8.5899 + 19.8\nu$ (Vs^{-1}) ($R^2 = 0.9978$) and confirm the inset figure. This indicates that a diffused controlled process controls the electron transfer reaction. A cyclic voltammetry signal for the oxidation of SFA appeared at the $SrWO_4$/PEDOT-PPy modified GCE to investigate the adsorption behavior of SFA, confirming that SFA was adsorbed during the oxidation process. This adsorption property enables the determination of SFA without interference from species like uric acid and dopamine. The presence of $SrWO_4$/PEDOT-PPy/GCE likely contributes to the adsorption of SFA/GCE.

In contrast, deviations from this expected electron count may suggest inefficiencies or side reactions occurring during the oxidation process, which could affect the overall catalytic performance of the hybrid material. Therefore, evaluating the correspondence between the expected and observed number of 2 electrons and 2 protons provides valuable insights into the functioning mechanism of SFA oxidation catalyzed by the hybrid nanocomposite (equation given below).

$$I = \frac{nFv}{4RT}$$

While, n is called as number of electrons, IPa is called as anodic peak current (μA), R is called as gas constant, T is called as temperature (K), F is called as faraday constant, Q

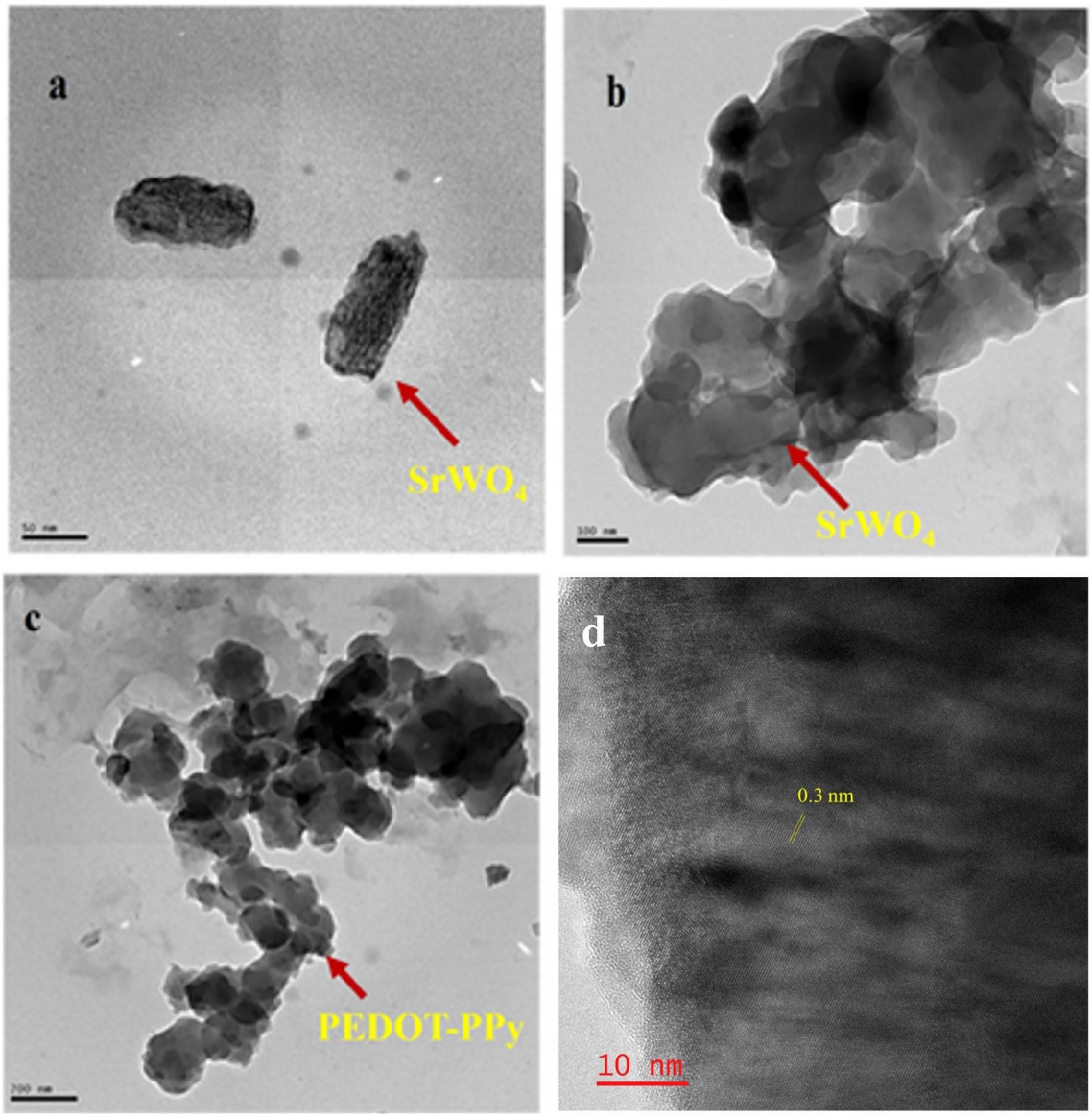

Fig. 6 **a**–**d** HR-TEM images of $SrWO_4$/PEDOT-PPy hybrids

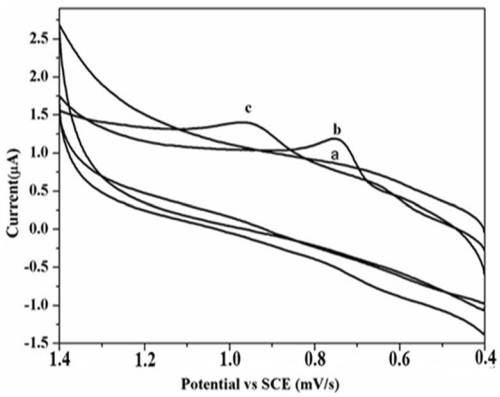

Fig. 7 CV investigation of $SrWO_4$/PEDOT-PPy/GCE in SFA: (**a**) pH—7, (**b**) GCE/SFA, (**c**) $SrWO_4$/PEDOT-PPy/GCE

is called as charge (C) and v is called as scan rate (mVs^{-1}) of the reaction.

Finally, rate constant (ks) and charge transfer coefficient (α) is also examined by the Laviron equation (dictated below).

$$Epc = E^{\circ} + (RT/\alpha nF)ln(RTk^{\circ}/\alpha nF) - (RT/\alpha nF)ln\upsilon$$

However, α is called as electron transfer coefficient, E^o is called as formal potential, R is called as gas constant (8.314 $J\ K^{-1}\ mol^{-1}$), n is called as number of transfer electron, F is called as Faraday's constant (96,485 C mol^{-1}), T is called as temperature (298 K), and k^o is called as standard rate constant respectively.

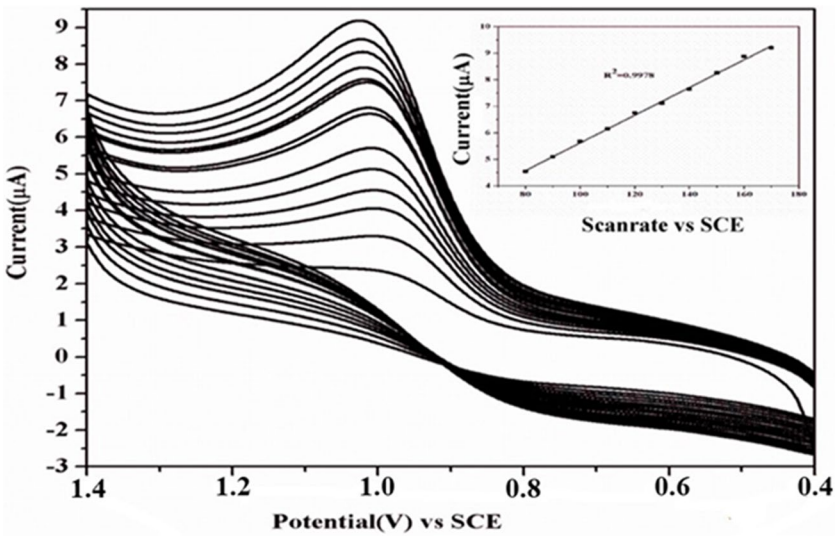

Fig. 8 Electrochemical analysis: $SrWO_4$/PEDOT-PPy/GCE in SFA at 50–180 mV/s scan rates. (Inserted figure is calibration plots of the modified electrodes.)

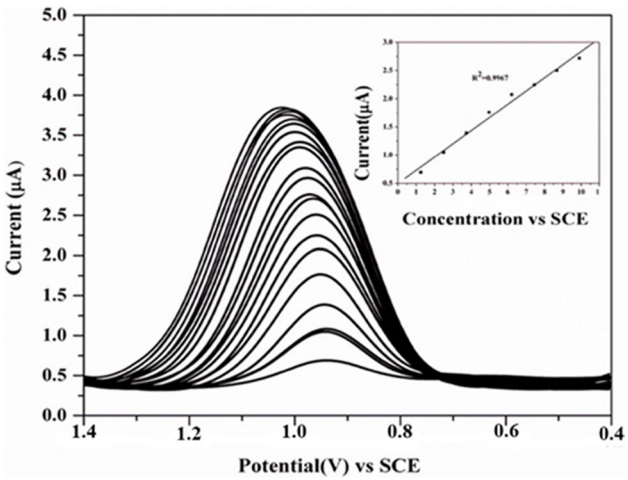

Fig. 9 a DPV analysis of $SrWO_4$/PEDOT-PPy/GCE in SFA (Inserted figure is calibrated plot of concentrations of 0. $1\times10^{-8}\sim10.5\times10.^{-9}$ M)

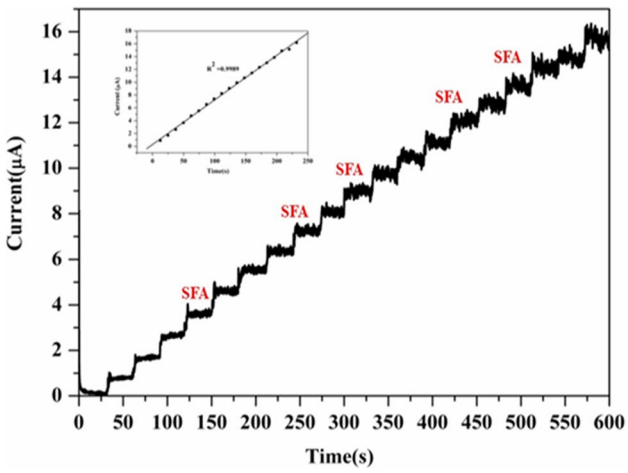

Fig. 10 a Amperometric analysis with calibrated plot of $SrWO_4$/PEDOT-PPy/GCE ($0.1\times10^{-5}\sim10.5\times10.^{-9}$ M)

DPV of SFA at $SrWO_4$/PEDOT-PPy/GCE

The DPV response of the $SrWO_4$/PEDOT-PPy modified GCE electrode demonstrates the promising potential for detecting SFA. As shown in Fig. 9, the DPV response exhibits a linear relationship with successive addition of SFA, indicating the ability to quantify SFA concentrations accurately. The calibration plot that was discussed in Fig. 9 **inset**, further confirms the linear DPV response over the concentration range tested. The linear DPV response range extends from 0.1×10^{-8} M to 10.5×10^{-9} M, and the sensitivity of the $SrWO_4$/PEDOT-PPy modified GCE is 3.502 μA/μM cm^{-2} underscores an electrode's ability to detect SFA at low concentrations. Additionally, the (QL) quantification limit, and (DL) detection limit values is 1.0936×10^{-9} M and 2.2104×10^{-9} M μA^{-1} which has indicated the electrode's capability to detect SFA at trace levels with satisfactory precision and accuracy. These results highlight the potential of the $SrWO_4$/PEDOT-PPy modified GCE, as a sensitive and reliable platform for the electrochemical detection of SFA.

Amperometric response of SFA at $SrWO_4$/PEDOT-PPy/GCE

The optimal electrode potential for chronoamperometric measurements to assess the stability and limit of detection of sulfadiazine (SFA) was determined to be 0.95 V versus saturated calomel electrode (SCE), using $SrWO_4$/PEDOT-PPy/modified GCE. These experiments were conducted under stirring conditions in 0.1 M phosphate buffer (pH 7), with the maintaining potential at 0.95 V versus time. Figure 10

shown significantly increases in the current response of SFA, while indicating the effective electrocatalytic oxidation. Moreover, the amperometry current response of the $SrWO_4$/PEDOT-PPy modified glassy carbon electrodes depend on various concentrations of SFA optimized for the potential. As the concentration of SFA also improved (ranges from 0.1×10^{-5} to 10.5×10^{-9} M), the oxidation current response also increased correspondingly. The calibration curve, depicted in the inset of Fig. 10, demonstrates a linear relationship with the equation I = 0.6950 (SFA) + 2.786 (c) and a high correlation coefficient of $R^2 = 0.9989$. Hence, we carried out results that are exhibiting an excellent sensitivity and low detection limits for sensing SFA. The morphologically favorable configuration, along with the synergistic effects and efficient capture of electrons, contributes to the enhanced performance of the proposed sensor for SFA detection.

Interference study of UA with DA of SFA at $SrWO_4$/PEDOT-PPy/GCE

Amperometric measurements were conducted to evaluate the response of the $SrWO_4$/PEDOT-PPy-modified glassy carbon electrode (GCE) to consecutive addition of 2 mM DA & 2 mM UA hip 0.1 M phosphate buffer solution on pH 7.0, maintaining peak potential at 0.95 V over time. Figure 11 illustrates the amperometric current response of the $SrWO_4$/PEDOT-PPy-modified GCE electrode to the sequential addition of 2 mM DA and 2 mM UA. Initially, different concentrations of sulfadiazine (SFA) (50, 100, 150 µL) were added and followed by the UA and DA (50, 100 µL), and then further additions of SFA. It is evident that the current increases upon the addition of SFA, while no significant response appeared for the addition of UA and DA. The catalytic current response of the SFA oxidation applied potential is 0.95 V. No current response is observed for UA and DA at this applied potential, indicating that 0.95 V is the optimized potential for sensing SFA. Furthermore, when UA and DA are measured alongside SFA, no significant current responses are obtained, highlighting the excellent efficiency of the freshly modified electrode in mitigating the interfering effects during the electroanalytical determination of SFA.

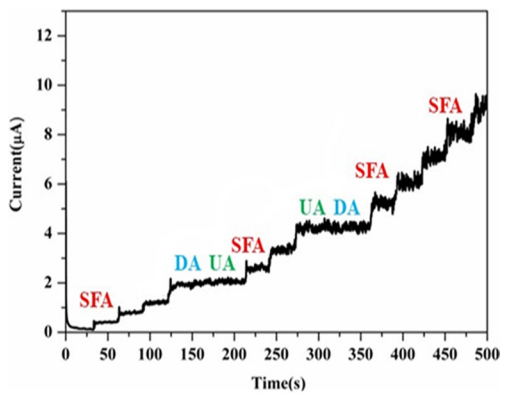

Fig. 11 **a** Amperometric analysis of $SrWO_4$/PEDOT-PPy/GCE/GCE in SFA, DA, and UA

Real sample analysis

Amperometric quantities of the SFA in the presence urine samples has directed to using standard adding methods towards deliberate the stabilities in $SrWO_4$/PEDOT-PPy modified GCE. Particularly, the actual samples (Urine) were diluted with UA. However, the SFA was arranged in urine samples to analyze urine samples in time. This present potential flow is 0.95 V with a slow magnetic sequence. An amperometric analysis of recently watery resolutions of actual samples (without SFA) revealed no current responses. Far ahead, the SFA was added, than sharpened in the sample, and detected in current responses. $SrWO_4$/PEDOT-PPy/GCE electrode shows an excellent recovery range of 99.5%. Based on this, as recovery results were shown in Table 1. $SrWO_4$/PEDOT-PPy/GCE demonstrations are respectable recoveries for the actual samples. These consequences promote the idea that future sensors can function as a capable and consistent stage for resolving SFA detection in urine samples.

Photodegradation of $SrWO_4$/PEDOT-PPy nanohybrid materials

Innovative oxidation processes offer promising solutions for addressing the environmental concerns of persistent organic pollutants in industrial wastewater. However, challenges persist in achieving efficient degradation of contaminants, particularly dyes, in wastewater treatment. Various catalysts have been explored for oxidative degradation, including metal oxides, metal oxychlorides, and dye activation, but generating reactive species for efficient dye oxidation remains a persistent challenge. Photocatalysis has emerged as a highly effective approach for the degradation and mineralization of manufacturing wastewater dyes owing to the subjects clean, sustainable, and stable characteristics. In photocatalytic degradation, photo-generated electron–hole pairs with solid oxidizing or reducing potentials are engendered within the catalyst surface's active sites. As

Table 1 Recovery results

Actual sample	Addition (µL)	Current (i Vs t)	Recovery (%)	RSD
UA	10	1.5	98.6	2.39
UA	20	3.1	97.4	2.71
UA	30	4.3	99.5	1.56

recombination rate of these photo-induced electron carriers is a crucial factor influencing the photocatalytic degradation efficiency of dyes like MB. Additionally, the redox ability also estimates by potentials of (CB) conduction band and (VB) valence band and its exposed photocatalytic degradation. Thereafter, the Poly(3,4-ethylenedioxythiophene)-polypyrrole (PEDOT-PPy) has occurred as a promising contender for photocatalytic applications due to its dual conjugation, metal-ion-free nature, low cost, and visible light response. However, the weak driving force of PEDOT-PPy arranged for photo-excited electron carriers are confines charge dynamics and degradation rates. To address this limitation, the creation of n-p type interfaces to modify charge dynamics and steer the activity of free radicals is required. Strontium tungstate ($SrWO_4$) provides ideal support for facilitating n-p type construction and enhancing the morphology, charge carrier dynamics, and electron transport of the $SrWO_4$/PEDOT-PPy structure. By forming n-p type double layers, $SrWO_4$-PEDOT-PPy exhibits improved degradation efficiency for dyes like methylene blue. By generating additional electron interfaces, introducing dopants such as camphor sulfonic acid (CSA) can enhance charge carrier separation and diffusion efficiency. The charge diffusion pathway follows a dual charge mechanism in the n-p type $SrWO_4$/PEDOT-PPy structure, contributing to efficient dye degradation.

Figure 12a depicts the absorption spectrum of a 5×10^{-3} M MB in $SrWO_4$/PEDOT-PPy catalyst, along with the time intervals. The dye absorption maximum is $\lambda = 663$ nm without any significant shift that appeared in absorption maximum. Initially, the absorbance of $SrWO_4$/PEDOT-PPy exhibited a maximum range higher for 0 min in before irradiation, which decreased after 10 min of irradiation. Then, continues irradiation for another 10 min and the absorbance maximum didn't change. Hence, the photocatalytic efficiency and rate constant ranges were examined by using absorbance value. Accordingly, the blank test has been proved by the MB dye with suffered insignificant self-degradation under dark medium for several minutes (Fig. 12b), while prescribed to a visible light degradation, which was not realized for the illumination. Furthermore, the test has been declared to the little self-degradation and contaminant

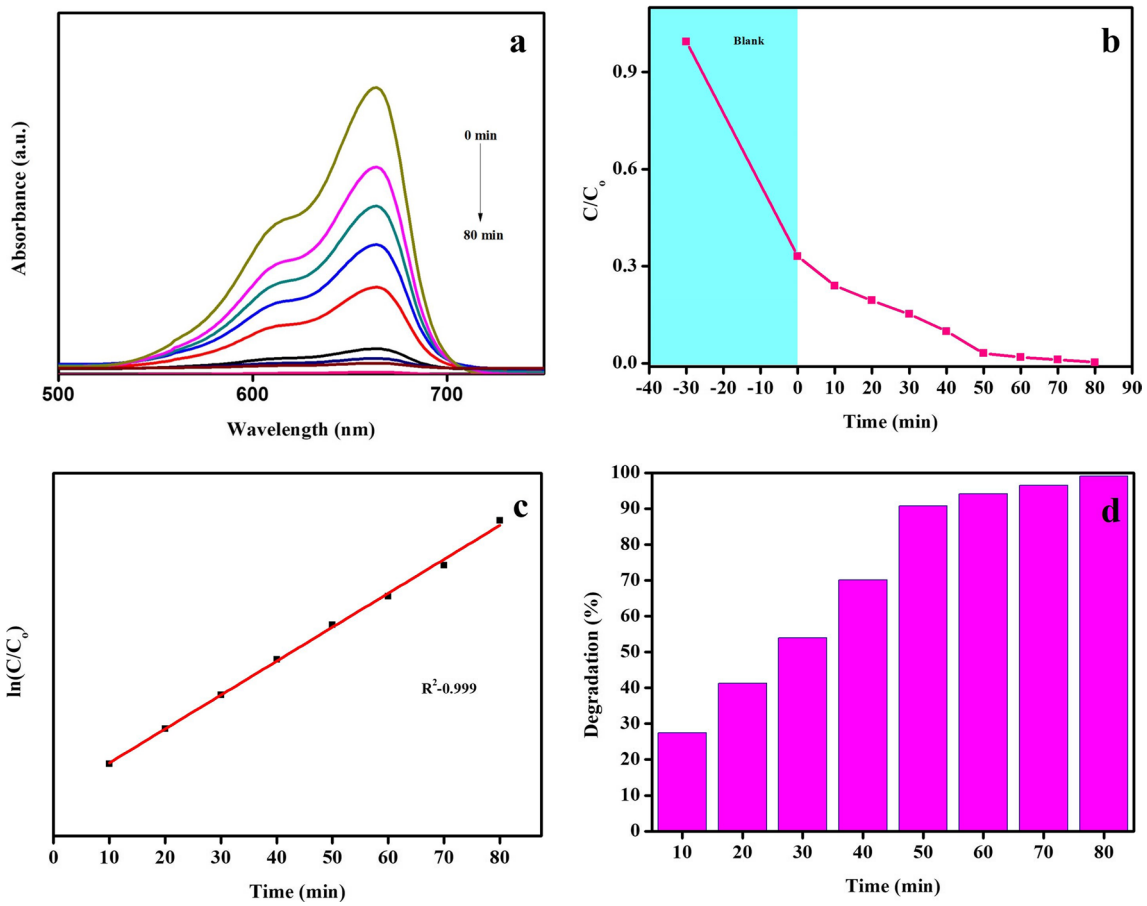

Fig. 12 **a–c** Photocatalytic activities (**a**) Absorption maximum MB, (**b**) Rate constants and (**c**) degradation efficiency of $SrWO_4$/PEDOT-PPy nanomaterials

impacts also none. This test has been followed by the other relevant articles (Gan et al. 2024; Manikandan et al. 2024).

Figure 12c presents the calculated decolonization efficiency of MB and $SrWO_4$/PEDOT-PPy nanoparticles demonstrated a maximum efficiency of 99.1%. The kinetic plot lnAt and irradiation time is shown in Fig. 12d**,** as considered rate constant values at R^2- 0.999 min^{-1}. Those results have indicated the good remarkable efficiency and effectiveness of $SrWO_4$/PEDOT-PPy nanohybrid materials. These $SrWO_4$/PEDOT-PPy nanohybrid materials have a giant degradation ability that should be compared to that of the other catalysts (El-Bindary et al. 2019; El-Dossoki et al. 2021; Awad et al. 2023).

The mechanism involves the generation of photo-induced holes (h^+) and electrons (e^-) by $SrWO_4$/PEDOT-PPy under visible light irradiation. Owing to the subordinate conduction band (CB), electrons from $SrWO_4$ may migrate to PEDOT-PPy, forming an n-p type configuration in the composite photocatalyst. This configuration enhances charge carrier separation and facilitates reactant transfer processes. Moreover, the interface between the d-orbitals of strontium tungsten oxide and the photocatalysts allows for the efficient departure of charge carriers, further improving MB adsorption on the photocatalyst surface. The free electrons react with O_2 crop superoxide radicals ($^{\bullet}O_2$), which combine with H_2O to $OH^{\bullet}$ radicals. The radicals initiate the degradation of MB into H_2O, CO_2, and other intermediates. The morphological transformation of $SrWO_4$/PEDOT-PPy significantly enhances the photocatalytic activity, stability, and reusability of the photocatalyst. Intentionally incorporating functional groups in $SrWO_4$/PEDOT-PPy, like NH assembly, contributes to its efficacy in MB degradation (Fig. 13). This mechanistic aspect has been followed by previous reported reports (Xu et al. 2024; Zhou et al. 2023, 2024a, 2024b; Lu et al. 2023; Xu et al. 2022; Ren et al. 2023; Lu et al. 2022; Cheng et al. 2024).

$$SrWO_4 - PEDOT - PPy + hv \rightarrow SrWO_4 - PEDOT - PPy + (e^-{}_{CB}{}^+ + h^+{}_{VB}) \quad (1)$$

$$SrWO_4 - PEDOT - PPy(e-_{CB}) + O_2 \rightarrow \bullet O_2 \quad (2)$$

$$SrWO_4 - PEDOT - PPy(h^+{}_{VB}) + H_2O \rightarrow SrWO_4 - PEDOT - PPy + H^+ + OH^{\bullet} \quad (3)$$

$$MB + {}^{\bullet}O_2 + OH^{\bullet} \rightarrow CO_2 + H_2O \quad (4)$$

Formation of hydroxyl radicals' investigations

The hydroxyl radical's determination study was carried out by the Fluorescence (PL) equipment. As an indicated procedure, 1 M terephthalic acid (TA) was dispersed in 2 mM NaOH solution with examined for reactor vessel and tested under 50 min. Meanwhile, 20 mg of the catalyst was supplementary in TA solution beneath magnetically stirring, collected every 10 min. As the same excitation was also used for the whole test. Furthermore, determined emission peak at 425 nm and fixed excitation range for 315 nm, these $OH^{\bullet}$ radicals formation undergoes the 2-hydroxyterephthalic acid, which have highly fluorescent behaviours (Li et al. 2022; Uribe-Lopez et al. 2021). This conversion has been examined and repeated for different time intervals. Figure 14 shows PL spectroscopy of the $SrWO_4$/PEDOT-PPy catalyst in the presence of TA, which improved the intensity and generates to the hydroxyl radicals.

Reusability confirmation study

The photocatalytic applications main backbone role and significant stricture for reusability, especially expected in well

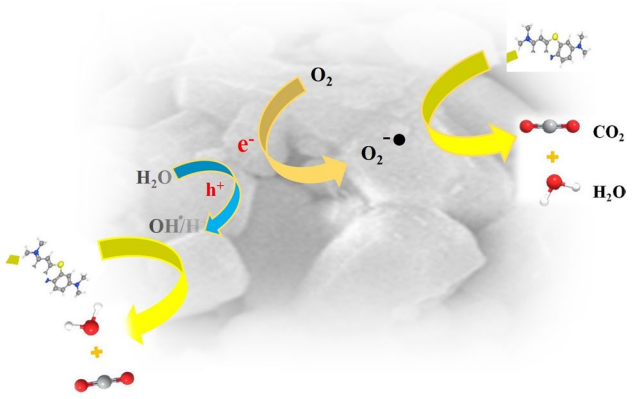

Fig. 13 Photocatalytic mechanism of MB in $SrWO_4$/PEDOT-PPy nanohybrids

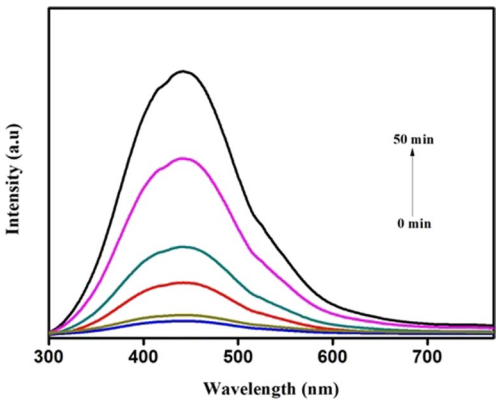

Fig. 14 Radical determination of MB in $SrWO_4$/PEDOT-PPy nanohybrids

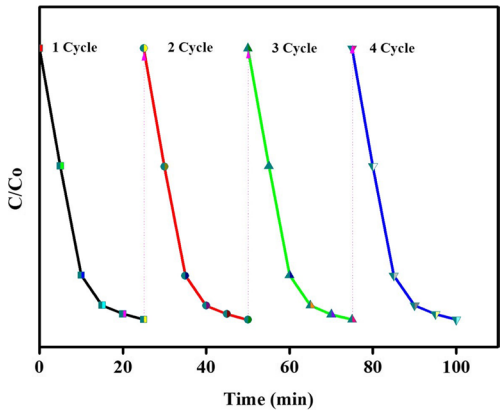

Fig. 15 Reusability activities of the $SrWO_4$/PEDOT-PPy nanohybrids

identity of the catalyst. However, these $SrWO_4$/PEDOT-PPy materials could be determined by the reusability measurements in the presence of the MB dye solution and it's followed by the simple method. This method is very feasible and reliable in a future correspondence application. The dye degradation of the $SrWO_4$/PEDOT-PPy nanohybrids catalyst with different time intervals has been demonstrated for various recycles are shown in Fig. 15**,** whose scrutinizing role is the optimization and completion of the illumination and maintenance at visible light. This same experiment was repeated several times and collected again for the catalyst maintained at 60℃ and resulted in pretty for the cycles. Therefore, this $SrWO_4$/PEDOT-PPy materials could be proven to be better beneficial approaches for the catalytic applications (Al Hunaiti et al. 2024; Vishwanathan et al. 2023; Wu et al. 2019; Cheng et al. 2018), the above-observed results didn't show any other significant difficulties, toxicity, loss, or any other kind of the issues so this nanocatalyst also refers as a good possibility nature of the degradation with recycle behaviours and environmental decades. The significant determinations were mentioned in the figure, which was designated to the photocatalytic enhancements.

Conclusion

In conclusion, the $SrWO_4$/PEDOT-PPy nanohybrids have been successfully achieved through a straightforward polymerization process, as confirmed by various analytical techniques, including UV–Visible DRS, FT-IR, FE-SEM, XRD, and HR-TEM. The $SrWO_4$/PEDOT-PPy nanocomposite tetragonal phase formation was confirmed by XRD, irregular cubes like morphological determination was carried out to the FE-SEM and HR-TEM investigations with observed diameter ranges at 200 to 50 nm. The M–O-M functional moieties were present in 459 to 814 cm^{-1} and other composites are confirmed by FT-IR spectroscopy. Rather than that, we can accomplish to 2.1 eV bandgap energy, such behaviours are acceptable for the different applications.

$SrWO_4$/PEDOT-PPy modified glassy carbon electrode (GCE) demonstrated excellent electrochemical performance for detecting SFA, exhibiting enhanced sensitivity compared to bare SFA. The detection limits (QL) and quantification limits (DL) for SFA detection were 1.0936×10^{-9} and 2.2104×10^{-9} M μA^{-1}, respectively, highlighting the sensor's high selectivity and sensitivity. Moreover, the $SrWO_4$/PEDOT-PPy nanohybrid showed promising potential as an electrocatalyst for developing cost-effective and efficient SFA electrochemical sensors for practical applications. Additionally, the hybrid material demonstrated excellent photocatalytic activity for MB degradation, achieved maximum efficiency of 99.1% for 80 min. This remarkable performance can be attributed to the inhibition of good recombination process, might be creation of the heterojunctions in between $SrWO_4$ and PEDOT-PPy hybrids. The main standards of the catalyst could be considered for a new ethnicity in the degradation, radical formations and good recyclable activities also examined. Comprehensively, the $SrWO_4$/PEDOT-PPy nanohybrid holds great promise not only for electrochemical sensing applications but also used for future photocatalytic applications in other pollutants and other viable potential impact for an environmental remediations.

Acknowledgements G. G, Z. L and other authors thank the School of Environment and Safety Engineering, Jiangsu University, Zhenjiang, Jiangsu, China, 212013.

Author contribution Gnanamoorthy Govindhan and Settu Munusamy—Writing original draft, Manuscript writing, Editing, Data's interpretation, Supervision; Correction Editing, Ziyang Lu—Supervision, Jie Jin—Formal investigation.

Funding K.M and D.A gratefully acknowledged the Centre for Computational Modelling, Chennai Institute of Technology, India, which has provided support by the following funding number CIT/CCM/2023 /RP-013.

Declarations

Competing interests The authors declare no competing interests.

References

Al Hunaiti A, Hamideh M, Al-Shawabkeh R (2024) Magnetic nanoparticles of TiO_2-$NiFe_2O_4$-Chitosan for photocatalytic degradation: synthesis, characterization, methyl blue dye - VOCs wastewater treatment, kinetic experimental, and theoretical studies. Emergent Mater 1-6

Alkaykh S, Mbarek A, Ali-Shattle EE (2020) Photocatalytic degradation of methylene blue dye in aqueous solution by $MnTiO_3$ nanoparticles under sunlight irradiation. Heliyon 6(4):03663

Altunay N (2022) Chemometric design-based optimization of a green, selective and inexpensive switchable hydrophilicity solvent-based liquid phase microextraction procedure for pre-concentration and

extraction of sulfadiazine in milk, honey and water samples. Food Chem 394:133540
Ammam M, Keita B, Nadjo L, Mbomekalle IM, Fransaer J (2010) Attempts to immobilize catalytically active substituted- heteropolytungstates in multilayer film of charged polyelectrolyte poly(allylamine hydrochloride). J Electroanal Chem 645:65
Awad ME, Farrag AM, El-Bindary AA, El-Bindary MA, Kiwaan HA (2023) Photocatalytic degradation of Rhodamine B dye using low-cost pyrofabricated titanium dioxide quantum dots-kaolinite nanocomposite. Appl Organomet Chem 37:e7113
Berdichevsky Y, Lo YH (2006) Polypyrrole nanowire actuators. Adv Mater 18:122
Bingyu X, Mingxia L, Kai P, Rong L, Naiying F, Guofeng W (2016) Synthesis, characterization and novel photoluminescence of $SrWO_4$:ln$_3$þ nanocrystals. J Nanosci Nanotech 16:3522
Bu X, Li J, Wang J, Li Y, Zhang G (2024) Boosting charge transfer promotes photocatalytic peroxymonosulfate activation of S-doped $CuBi_2O_4$ nanorods for ciprofloxacin degradation: Key role of Ov–Cu–S and mechanism insight. Chem Eng J 494:153075
Cavalcante LS, Sczancoski JC, Batista NC, Longo E, Varela JA (2013) Orlandi, Growth mechanism and photocatalytic properties of $SrWO_4$ microcrystals synthesized by injection of ions into a hot aqueous solution. Adv Powder Technol 24:344–353
Chen D, Liu Z, Ouyang S, Ye J (2011) Simple room-temperature mineralization method to $SrWO_4$ micro/nanostructures and their photocatalytic properties. J Phys Chem C 115:15778
Cheng J, Wang X, Zhang Z et al (2018) Synthesis of flower-like Bi_2O_4/ZnO heterojunction and mechanism of enhanced photodegradation for organic contaminants under visible light. Res Chem Intermed 44:6569–6590
Cheng Q, Wang Z, Wang X, Li J, Li Y, Zhang G (2023) A novel $Cu_{1.5}Mn_{1.5}O_4$ photothermal catalyst with boosted surface lattice oxygen activation for efficiently photothermal mineralization of toluene. Nano Res 16(2):2133–2141
Cheng Y, Jin J, Yan H, Zhou G, Xu Y, Tang L, Liu X, Li H, Zhang K, Lu Z (2024) Spaced double hydrogen bonding in an imidazole poly ionic liquid composite for highly efficient and selective photocatalytic air reductive H_2O_2 synthesis. Angew Chem Int Ed 63:e202400857
Chougule MA, Pawar SG, Godse PR, Mulik RN, Sen S, Patil VB (2011) Synthesis and characterization of Polypyrrole (PPy) thin films. Soft Nanoscience Letters 1:6–10
De Armit C, Armes SP (1993) Colloidal dispersions of surfactant stabilized polypyrrole particles. Langmuir 9:652
Duraimurugan J, Kumar GS, Venkatesh M, Maadeswaran P, Girija EK (2018) Morphology and size-controlled synthesis of zinc oxide nanostructures and their optical properties. J Mater Sci Mater Electron 29:9339–9346
Eftekhari A, Kazemzad M (2006) Significant effect of dopant size on nanoscale fractal structure of polypyrrole film. Polymer J 38:781
El-Bindary AA, El-Marsafy SM, El-Maddah AA (2019) Enhancement of the photocatalytic activity of ZnO nanoparticles by silver doping for the degradation of AY99 contaminants. J Mol Struct 1191:76–84
El-Dossoki FI, Atwee TM, Hamada AM, El-Bindary AA (2021) Photocatalytic degradation of Remazol Red B and Rhodamine B dyes using TiO_2 nanomaterial: estimation of the effective operating parameters. Desalin Water Treat 233:319–330
Gan G, Yang Z, Li Y, Zhang G (2024) Efficient photothermal mineralization of toluene over $MnCo_2O_4$ with different exposed facets: revealing the role of oxygen vacancy and photo-/thermo-synergistic mechanism. Appl Catal b: Environ 357:124308
Gnanamoorthy G et al (2020) Enhanced photocatalytic performance of $ZnSnO_3$/rGO nanocomposite. Chem Phys Lett 739:137050
Gnanamoorthy G, Karthikeyan V, Ali D, Kumar G, Yadav VK, Narayanan V (2022) Global popularization of $CuNiO_2$ and their rGO nanocomposite loveabled to the photocatalytic properties of methylene blue. Environ Res 204:112338
Gnanamoorthy G, Yadav VK, Jin J, Munusamy S, Narayanan V, Lu Z (2024a) New amendment of VO_2 nanoparticles with enhanced photocatalytic and antibacterial activities. BioNanoScience. https://doi.org/10.1007/s12668-024-01312-4
Gnanamoorthy G, Jin J, Yadav VK, Narayanan V, Lu Z (2024b) Novel zirconium aminophosphates nanowires and superior photocatalytic activities under visible light degradation. Optik 300:171631
Goren M, Lennox RB (2001) Nanoscale polypyrrole patterns using block copolymer surface micelles templates. Nano Lett 12:735
Groenendaal L, Freitag D, Pielartzik H, Jonas F (2000) Poly(3,4 ethylenedioxythiophene) and its derivatives past present and future. Adv Mater 12:481
Herrmann S, Ritchie C, Streb C (2015) Polyoxometalate–conductive polymer composites for energy conversion, energy storage and nanostructured sensors. Dalt Trans 44:7092
Jang J, Yoon H (2005) Formation mechanism of conducting polypyrrole nanotubes in reverse micelle systems. Langmuir 21:11484
Jayakrishnan C, Sheeja SR, Kumar GS, Lalithambigai K, Duraimurugan J, Alam MM (2024) Hydrothermal assisted synthesis of shape-controlled zinc oxide nanostructures for tuneable photodegradation of methylene blue pollutant. J Sol-Gel Sci Technol. https://doi.org/10.1007/s10971-024-06515-5
Jia T-Z et al (2024) Conductive nanofiltration membranes via in situ PEDOT-polymerization for electro-assisted membrane fouling mitigation. Water Res 252:121251
Jiandong F, Huaijin Z, Zhengping W, Wenwei G, Jiyang W (2006) Synthesis of polycrystalline materials of $SrWO_4$ and growth of its single crystal. Front Chem China 3:264
Kang TS, Lee SW, Joo J, Lee JY (2005) Electrically conducting polypyrrole fibers spun by Electrospinning. Synth Met 153:61
Kang SK, Kim JH, An J, Lee EK, Cha J, Lim G, Park YS, Chung DJ (2024) Synthesis of polythiophene derivatives and their application for electrochemical DNA sensor. Polym J 36:937
Karlsson KF, Aasberg P, Nilsson KPR, Inganaes O (2005) Interaction between a zwitterionic polythiophene derivative and oligonucleotides as resolved fluorescence resonance energy transfer. Chem Mater 17:4204
Kokulnathan T (2021) Elumalai Ashok Kumar, Tzyy-Jiann Wang, Chiang Cheng, Strontium tungstate-modified disposable strip for electrochemical detection of sulfadiazine in environmental samples. Ecotoxicol Environ Saf 208:111516
Kumar A, Kumar D, Pandey G (2016) Characterisation of hydrothermally synthesised CuO nanoparticles at different pH. JTASR 4:166
Li W, Wang Z, Li Y, Ghasemi J, Li J, Zhang G (2022) Visible-NIR light-responsive 0D/2D CQDs/Sb_2WO_6 nanosheets with enhanced photocatalytic degradation performance of RhB: Unveiling the dual roles of CQDs and mechanism study. J Hazard Mater 424:124308
Lu Z, Zhou G, Li B, Yangrui Xu, Wang P, Yan H, Song M, Ma C, Han S, Liu X (2022) Heterotopic reaction strategy for enhancing selective reduction and synergistic oxidation ability through trapping Cr (VI) into specific reaction site: a stable and self-cleaning ion imprinted CdS/HTNW photocatalytic membrane. Appl Catal b: Environ 301:120787

Lu Z, Li B, Wei B, Zhou G, Yangrui Xu, Zhang J, Chen H, Hua S, Chundu Wu, Liu X (2023) NMP-induced surface self-corrosion-assisted rapid spin-coating method for synthesizing imprinted heterojunction photocatalyst anchored membrane towards high-efficiency selective degradation tetracycline. Sep Purif Technol 314:123609

Manikandan V et al (2024) Chemically engineered CoOx-doped flower-like NiO nanoparticles for photodegradation of Bisphenol A and Orange II Dye, and genetic screening of toxicity via Caenorhaditis elegans. J Environ Chem Eng 12:113677

Moztahida M, Lee DS (2020) Photocatalytic degradation of methylene blue with P25/ graphene/polyacrylamide hydrogels: optimization using response surface methodology. J Hazard Mater 400:123314

Munusamy S, Suresh R, Giribabu K, Manigandan R, Kumar SP, Muthamizh S, Bagavath C, Stephen A, Kumar J, Narayanan V (2019) Synthesis and characterization of GaN/PEDOT–PPY nanocomposites and its photocatalytic activity and electrochemical detection of mebendazole. Arab J Chem 12:3565–3575

Otero TF, Cortes MT (2003) Artificial muscles with tactile sensitivity. Adv Mater 16:279

Parthasarathy A, Brumlik CJ, Martin CR, Collins GE (1994) Interfacial polymerization of thin polymer films onto the surface of a micro porous hollow fiber membrane. J Membr Sci 94:249

Peng C, Jin J, Chen GZ (2007) A comparative study on electrochemical co deposition and capacitance of composite films of conducting polymers and carbon nanotubes. Electrochim Acta 53:525

Pringle JM et al (2004) Electrochemical synthesis of polypyrrole in ionic liquids. Polymer 45(5):1447–1453

Raja VR, Karthika A, Lok Kirubahar S, Suganthi A, Rajarajan M (2019) Sonochemical synthesis of novel $ZnFe_2O_4/CeO_2$ heterojunction with highly enhanced visible-light photocatalytic activity. Solid State Ion 332:55

Rajkumar S, Dhineshkumar S, Arunprakash N, Raychel P, Kumar SA, Merlin JP (2023) Fabrication of $SrWO_4$/PPy composite as electrode material for high-performance supercapacitors. Opt Mater 142:113934

Ramanavicius A, Malinauskas A (2006) Electrochemical sensors based on conducting polymers polypyrrole. Electrochim Acta 51:6025

Ren Y, Zhou G, Ziyang Lu (2023) Utilization of porous liquids for catalytic conversion. Chinese J Struc Chem 42:100045

Rendón-Angeles JC, Matamoros-Veloza Z, López-Cuevas J, Gonzalez LA, Montoya-Cisneros KL, Yanagisawa K, Willis-Richards J, Diaz-Algara J (2015) Rapid synthesis of scheelite $SrWO_4$ particles using a natural $SrSO_4$ ore under alkaline hydrothermal conditions. Hydrometallurgy 157:116–126

Sczancoski JC, Cavalcante LS, Joya MR, Espinosa JWM, Pizani PS, Varela JA, Longo E (2009) Synthesis, growth process and photoluminescence properties of $SrWO_4$ powders. J Colloid Interface Sci 330:227–236

Shi Y, Wang J, Li S, Yan B, Xu H, Zhang K, Du Y (2017) The enhanced photoelectrochemical detection of uric acid on Au nanoparticles modified glassy carbon electrode. Nanoscale Res Lett 12:455

Shim GH, Han MG, Sharp-Norton JC, Creager SE, Foulger SH (2008) Inkject –printed electrochromic devices utilizing polyaniline-silica and poly(3,4 ethylenedioxythiophene)-silica colloidal composite particles. J Mater Chem 18:594

Shivakumara C, Saraf R, Behera S, Dhananjaya N, Nagabhushana H (2015) Scheelite-type MWO_4 (M = Ca, Sr, and Ba) nanophosphors: facile synthesis, structural characterization, photoluminescence, and photocatalytic properties. Mater Res Bull 61:422–432

Shuying Y, Stephen M (2006) Analysis of the 1030 cm^{-1} band of poly(ethylene terephthalate) fibers using polarized Raman microscopy. J Polym Sci, Part B: Polym Phys 47:42

Suda J, Zverev PG (2019) Temperature dependence of Raman frequency shift in $SrWO_4$ crystal studied by lattice dynamical calculations. Crystals 9:197

Uribe-Lopez MC et al (2021) Photocatalytic activity of ZnO nanoparticles and the role of the synthesis method on their physical and chemical properties. J Photochem Photobiol A 404:112866

Vishwanathan S, Laxmi S, Nandan S, Jayan S, Lijo M, Das S (2023) Efect of experimental parameters on photocatalytic degradation efficiency of TiO_2 nanoparticles synthesized by electrochemical method towards Rhodamine B dye solution under natural sunlight. Environ Sci Pollut Res 30:8448–8463

Vito SD, Martin CR (1998) Toward colloidal dispersions of template synthesized polypyrrole nanotubules. Chem Mater 10:1738

Wallace GG, Kane-Maguire LAP (2002) Manipulating and monitoring biomolecular interactions with conducting electroactive polymers. Adv Mater 14:53

Wang J, Jiang M (2000) Toward genolelectronics nucleic acid doped conducting polymers. Langmuir 16:2269

Wang J, Martin CR (1996) Nanotube membranes for biotechnology in nanobiotechnology; bioinspired devices and materials. J Mater Chem 8:2382

Wang D, Zhang D, Pan Q, Wang T, Chen F (2022) Gas sensing performance of carbon monoxide sensor based on rod-shaped tin diselenide/MOFs derived zinc oxide polyhedron at room temperature. Sensor Actuator B Chem 371:132481

Wu A, Kolla HS, Manohar SK (2005) Chemical synthesis of highly conducting polypyrrole nanofiberfilm. Macromolecules 38:7873

Wu Z, Che X, Liu X, Yang X, Yang Y (2019) A ternary magnetic recyclable $ZnO/Fe_3O_4/g\text{-}C_3N_4$ composite photocatalyst for efficient photodegradation of monoazo dye. Nanoscale Res Lett 14:147

Xu Y, Zhu X, Yan H, Wang P, Song M, Ma C, Chen Z, Chu J, Liu X, Ziyang Lu (2022) Hydrochloric acid-mediated synthesis of $ZnFe_2O_4$ small particle decorated one-dimensional PDI S-scheme heterojunction with excellent photocatalytic ability. CHINESE J CATAL 43:1111

Xu Y, Ren Y, Zhou G, Feng S, Yang Z, Dai S, Lu Z, Zhou T (2024) Amide-engineered metal-organic porous liquids toward enhanced CO_2 photoreduction performance. Adv Funct Mater 34(19):2313695

Yang Ting et al (2024) Interfacial polymerization of PEDOT sheath on V_2O_5 nanowires for stable aqueous zinc ion storage. J Mater Chem A 12(17):10137–10147

Yu X, Yang Y, Shen Q, Sun Y, Kang Q, Shen D (2024) A novel differential ratiometric molecularly imprinted electrochemical sensor for determination of sulfadiazine in food samples. Food Chem 434:137461

Zhang X, Manohar SK (2004) Bulk synthesis of polypyrrole nanofibers by a seeding approach. J Am Chem Soc 126(40):12714

Zhang L, Wan M, Wei Y (2006) Nano scaled polyaniline fibers prepared by ferric chloride as an oxidant. Macromol Rapid Commun 27:366

Zhang Li, Jamal R, Zhao Q, Wang M, Abdiryim T (2015a) Preparation of PEDOT/GO, PEDOT/MnO_2, and PEDOT/GO/MnO_2 nanocomposites and their application in catalytic degradation of methylene blue. Nanoscale Res Lett 10:148

Zhang Y, Li L, Su H, Huang W, Dong X (2015b) Binary metal oxide: advanced energy storage materials in supercapacitors. J Mater Chem A 3:43–59

Zhou G, Yangrui Xu, Cheng Yu, Zehui Yu, Wei B, Liu X, Chen Z, Li C, Ziyang Lu (2023) Rapid dissociation of high concentration excitons between $[Bi_2O_2]^{2+}$ slabs with multifunctional N-Bi-O sites for selective photoconversion into CO. Appl Catal b: Environ 335:122892

Zhou G, Liu X, Xu Y, Feng S, Lu Z, Liu Z-Q (2024a) Enhancing d/p-2π orbitals hybridization via strain engineering for efficient photoreduction CO_2. Angew Chem Int Ed e202411794

Zhou G, Yangrui Xu, Wang P, Liguang Tang Yu, Cheng JJ, Ma Z, Liu X, Li C, Ziyang Lu (2024b) Homogenization spin coating strategy for synthesizing IM-BTO photocatalytic membrane aims to tetracycline selectively degradation. Chem Eng J 486:150163